Stokes–anti-Stokes correlations in diamond

Mark Kasperczyk,[1] Ado Jorio,[2] Elke Neu,[3] Patrick Maletinsky,[3] and Lukas Novotny[1,*]

[1]*Photonics Laboratory, ETH Zürich, 8093 Zürich, Switzerland*

[2]*Departamento de Física, Universidade Federal de Minas Gerais, Belo Horizonte, MG 30123-970, Brazil*

[3]*Department of Physics, University of Basel, Klingelbergstrasse 82, Basel CH-4056, Switzerland*

**Corresponding author: lnovotny@ethz.ch*

Received March 23, 2015; accepted April 23, 2015;
posted April 28, 2015 (Doc. ID 236585); published May 14, 2015

We investigate the arrival statistics of Stokes (S) and anti-Stokes (aS) Raman photons generated in thin diamond crystals. Strong quantum correlations between the S and aS signals are observed, which implies that the two processes share the same phonon; that is, the phonon excited in the S process is consumed in the aS process. We show that the intensity cross-correlation $g^{(2)}_{\mathrm{S,aS}}(0)$, which describes the simultaneous detection of Stokes and anti-Stokes photons, increases steadily with decreasing laser power and saturates at very low pump powers, implying that the number of Stokes-induced aS photons is comparable to the number of spontaneously generated aS photons. Furthermore, the coincidence rate shows a quadratic plus cubic power dependence, indicating the generation of multiple S photons per pulse at high powers. © 2015 Optical Society of America

OCIS codes: (290.5860) Scattering, Raman; (190.4180) Multiphoton processes; (270.5290) Photon statistics; (160.4760) Optical properties.

http://dx.doi.org/10.1364/OL.40.002393

Raman scattering, typically used to probe the vibrational modes of a system, can also create correlated Stokes–anti-Stokes photon pairs in bulk solids such as diamond [1–3] or in gases such as Cesium [4,5] or Rubidium vapor [6–8]. In the uncorrelated regime, both Stokes (S) and anti-Stokes (aS) intensities are linear with excitation laser power, i.e., a single laser photon spontaneously scatters into a single S or aS photon [see Fig. 1(a)]. However, if the phonon energies are high enough that the thermal phonon occupation is low, the spontaneous aS process is rare and correlations between S and aS photon generation set in [see in Fig. 1(b)]. In this case, we expect that the aS intensity depends on the squared excitation laser power, since one laser photon creates the phonon in the S process, and another laser photon scatters from the phonon in the aS process [9,10]. Recent work has shown theoretically and experimentally that the Stokes-generated phonon (or spin wave, for Cesium [4,5] and Rubidium vapors [6–8]) acts as a quantum memory, where the S and aS signals act as write and read commands [1–3,9]. In parallel, research in photon pairs produced through four-wave mixing (FWM) in optical fibers has shown highly nonclassical correlations [11,12], analogous to studies in spontaneous parametric down-conversion (SPDC) [13,14]. Entanglement between photon pairs generated through FWM in Rubidium vapors has also been demonstrated [15]. However, whereas SPDC and FWM are broadband processes, here the S and aS energies are determined by the phonon energy. The Stokes–anti-Stokes (SaS) process is thus a version of coherent anti-Stokes Raman scattering (CARS) in which the beam at the S wavelength is generated spontaneously in the material.

In Lee *et al.*, nonclassical correlations between S and aS photons in diamond were observed, but superbunching was never achieved, and the correlations were observed for only a single pump power [1]. In this Letter, we report the generation of highly nonclassical photon superbunching in diamond at low excitation powers and analyze Stokes–anti-Stokes photon correlations as a function of pump power. Our data reveal the range of conditions under which Stokes-induced anti-Stokes scattering (SaS) can be used to generate correlated photons in diamond. This information is useful for designing efficient phonon-based quantum memories and heralded single-photon sources for quantum communication. Contrary to FWM in optical fibers [11] and SPDC in nonlinear crystals [13], we observe a saturation of Stokes–anti-Stokes correlations at very low intensities.

Here we measure Stokes and anti-Stokes photons in diamond as a function of laser power P_L. Our setup for measuring correlations between S and aS photons is illustrated in Fig. 2(a). The excitation wavelength is $\lambda = 785$ nm from a Ti:Sapph laser, and the Stokes and anti-Stokes photons appear at the wavelengths $\lambda_{\mathrm{S}} = 877$ nm and $\lambda_{\mathrm{aS}} = 711$ nm, respectively, as defined by the phonon frequency of 1332 cm^{-1} in diamond [1]. The duration of the excitation laser pulses is $\tau = 130$ fs, with a repetition rate of $\Delta f = 76$ MHz. The sample is a free-standing 50-μm-thick diamond crystal, suspended over a 3-mm-diameter hole in a 1.5-mm-thick quartz substrate. As shown in Fig. 2(b), the S signal shows a linear power dependence, whereas the aS signal exhibits a quadratic power dependence at high intensities, as predicted for

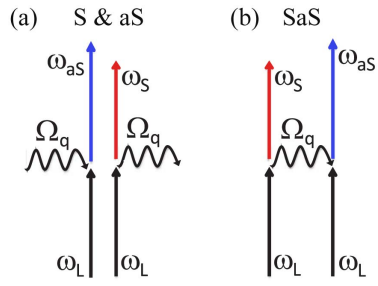

Fig. 1. Schematic representation of Stokes (S) and anti-Stokes (aS) Raman scattering. (a) Uncorrelated (i.e., spontaneous) S and aS processes (S & aS). The phonons responsible for the aS process are generated thermally. (b) Anti-Stokes photons can also be generated by the phonons created through the Stokes process. Stokes photons and Stokes-induced anti-Stokes (SaS) photons become correlated.

 © 2015 Optical Society of America

the SaS process illustrated in Fig. 1(b) [10]. At low powers, on the other hand, the spontaneously generated aS process is comparable to the SaS process, and hence the aS signal deviates from the quadratic dependence.

We also record histograms of the difference in arrival times between S and aS photons. The S and aS photons are detected at a pair of APDs in free space, and we send the APD pulses to the "start" and "stop" inputs of a commercial time-correlated single-photon counting (TCSPC) system. A representative coincidence histogram is shown in Fig. 3(a). The coincidence rate is calculated by dividing the coincidence counts at time delay $\Delta t = 0$ by the measurement time, where Δt represents the difference in arrival times between the S and aS photons. Thus $\Delta t = 0$ represents the simultaneous arrival of one Stokes and one anti-Stokes photon, within the experimental binning time of 4 ps. The accuracy of the measurement is limited by the timing uncertainty ($\lesssim$50 ps) of the APDs.

The coincidence rate can be written in terms of probabilities of generating Stokes and anti-Stokes photons. The product rule allows the probability of measuring a Stokes–anti-Stokes pair $P(\mathrm{S}, \mathrm{aS})$ to be rewritten as

$$P(\mathrm{S}, \mathrm{aS}) = P(\mathrm{aS}|\mathrm{S})P(\mathrm{S}) = P(\mathrm{S}|\mathrm{aS})P(\mathrm{aS}), \qquad (1)$$

where $P(\mathrm{aS}|\mathrm{S})$ denotes the conditional probability of detecting an anti-Stokes photon given that a Stokes photon has already been detected, and similarly for $P(\mathrm{S}|\mathrm{aS})$

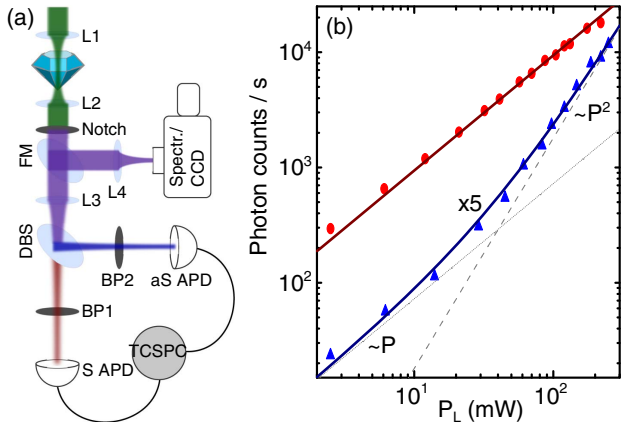

Fig. 2. (a) Experimental setup. A 0.5-NA objective (L1) focuses 785-nm linearly polarized light (shown in green) on a 50-μm-thick diamond sample. The scattered light is collected with a 0.9-NA air objective (L2). A notch filter blocks the excitation light. The light is sent either to a spectrometer and CCD (using a flip mirror FM) or to a pair of avalanche photodiodes (APD) in free space. A dichroic beamsplitter (DBS) separates the S (red) and aS (blue) signals, sending them to separate APDs. Bandpass filters BP1 and BP2 block all remaining light except at the S and aS wavelengths, respectively. A TCSPC system creates histograms of relative arrival times between S and aS photons. (b) Dependence of Stokes signal (red circles) and anti-Stokes signal (blue triangles) on average excitation power measured in the forward direction. The data points are the area of Gaussian fits to the spectral lines, normalized by the integration time. The Stokes signal is linear with laser power, whereas the anti-Stokes signal shows a linear power dependence for low laser powers and quadratic dependence for high laser powers. The aS data and fit have been multiplied by a factor of 5 to show it on the same scale as the S data. The gray lines are the linear (dotted) and quadratic (dashed) parts of the aS fit.

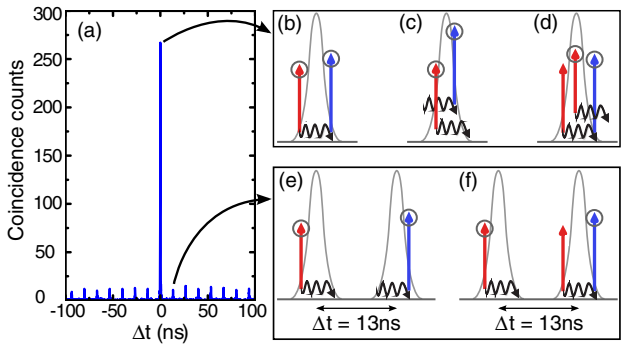

Fig. 3. (a) A typical coincidence histogram. Count rates for this experiment were 4.2 kHz for Stokes and 200 Hz for anti-Stokes. The average incident power was 8.6 mW. (b),(c), and (d) show the contributions to the peak at $\Delta t = 0$. Red (blue) arrows indicate Stokes (anti-Stokes) photons, and the wavy black lines are phonons. The gray circles show which photons are detected and thereby contribute to the measured coincidences. (b) True coincidences, corresponding to the process from Fig. 1(b). (c) Accidental coincidences from spontaneous aS. (d) Accidental coincidences from generating multiple S photons per pulse. (e) and (f) show the accidental coincidences between different pulses, taking the peak at $\Delta t = 13$ ns as an example. (e) A S photon is generated in one pulse, and an aS photon is generated spontaneously in the pulse immediately following. Since the S and aS photons are separated by one pulse, the TCSPC bins this accidental coincidence into the peak near $\Delta t = 13$ ns. (f) Accidental coincidences due to the generation of a S photon in one pulse and a Stokes-induced aS photon in the subsequent pulse.

[1]. $P(\mathrm{S})$ and $P(\mathrm{aS})$ are the unconditional probabilities for detecting Stokes and anti-Stokes photons. The two primary contributions to the total coincidence rate are from the Stokes-induced aS [P_{corr}, due to correlated coincidences shown in Fig. 3(b)] and spontaneously generated aS [P_{acc}, due to accidental coincidences shown in Fig. 3(c)]. Note that the accidental coincidences are independent of time delay, i.e., the probability of Fig. 3(c) is equal to that of Fig. 3(e), and similarly for Figs. 3(d) and 3(f). In the absence of thermal phonons, $P(\mathrm{S}|\mathrm{aS})$ is given by the collection and detection efficiency η_{S} at the Stokes frequency [9]. In other words, detection of an anti-Stokes photon requires that a Stokes photon was created, though it may be undetected. The power dependence of the coincidences is therefore determined by the power dependence of the anti-Stokes signal, that is, $P_{\mathrm{corr}}(\mathrm{S}, \mathrm{aS}) = \eta_{\mathrm{S}} P(\mathrm{aS})$. In the absence of thermal phonons, the anti-Stokes signal scales quadratically with laser power P_L (see Fig. 2) and hence $P_{\mathrm{corr}}(\mathrm{S}, \mathrm{aS}) \propto P_L^2$, which agrees with our coincidence measurements shown in Fig. 4(a). Note, however, that spontaneously generated coincidences also exhibit a quadratic power dependence. In this case, Stokes and anti-Stokes processes are independent, that is, $P(\mathrm{S}|\mathrm{aS}) = P(\mathrm{S})$, and hence $P_{\mathrm{acc}}(\mathrm{S}, \mathrm{aS}) = P(\mathrm{S})P(\mathrm{aS}) \propto P_L^2$. Contrary to the SaS process, spontaneous coincidences are independent of time delay Δt. Thus the total coincidence rate alone gives no information about the degree of correlation. We must account for accidental coincidences as well.

At high pump powers ($P_L > 150$ mW), we observe the onset of a cubic term in the coincidence rate. Here the

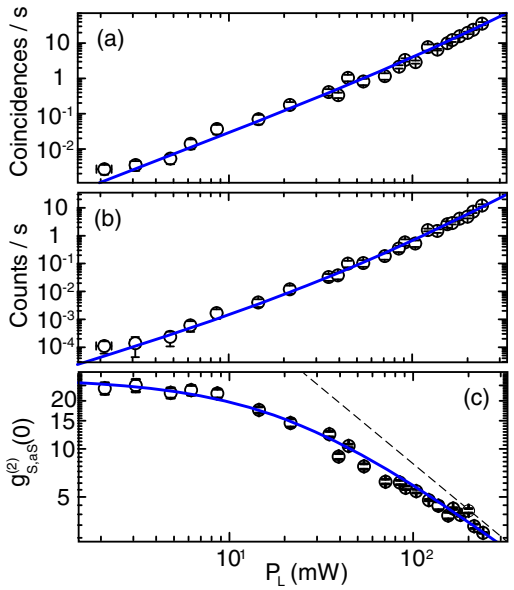

Fig. 4. Correlation of Stokes and anti-Stokes photons as a function of laser power. (a) Total coincidence rate at $\Delta t = 0$. The fitting curve is quadratic for low P_L and cubic for high P_L. (b) Accidental coincidence rate, given by the peaks at $\Delta t \neq 0$. (c) Second-order correlation for zero time delay $g^{(2)}_{S,aS}(0)$. The dashed line indicates the theoretical $1/P_L$ behavior. At low powers, $g^{(2)}_{S,aS}(0)$ stops increasing because the yield of Stokes-induced anti-Stokes photons becomes comparable to that of spontaneously generated anti-Stokes photons.

probability of generating multiple phase-matched phonons per pulse is no longer negligible. The cubic dependence arises from detecting a S photon followed by an aS photon generated through a second S photon, i.e., two S photons and one aS photon in the same pulse. Since this requires the creation of an additional S photon, the probability scales as P_L^3 [see Fig. 3(d)].

To understand the interplay between the spontaneous and the Stokes-induced aS processes, we measure the second-order intensity cross-correlation $g^{(2)}_{S,aS}(0)$ as a function of average laser power. Using the recorded histograms, we can evaluate $g^{(2)}_{S,aS}(0)$ by dividing the total coincidences at $\Delta t = 0$ by the average accidental coincidences taken from the peaks at $\Delta t \neq 0$. The phonon lifetime in diamond is ≈3.6 ps, which determines the lifetime of the cross-correlations between the S and aS signals [1]. The separation between pulses (given by the laser repetition rate) is 13 ns. It is thus unlikely that a phonon generated in one pulse survives until the subsequent pulse, implying that correlations should only exist for S and aS photons generated within the sample pulse, i.e., at $\Delta t = 0$. Thus the peaks at $\Delta t \neq 0$ represent accidental coincidences, i.e., S and aS photons that are generated in different pulses and are therefore uncorrelated [see Figs. 3(e) and 3(f)].

Classically, $g^{(2)}_{S,aS}(0)$ is related to the autocorrelations through the inequality $g^{(2)}_{S,aS}(0) \leq \sqrt{g^{(2)}_{S,S}(0) g^{(2)}_{aS,aS}(0)}$ [1,16]. The autocorrelations are classically bound by $g^{(2)}_{S,S}(0)$, $g^{(2)}_{aS,aS}(0) \leq 2$, where the equality holds for the thermal state of a single-mode field [1,16]. For a large range of intensities, our value of $g^{(2)}_{S,aS}(0)$ violates the inequality since the photon arrival statistics cannot be described classically. Specifically, the value of $g^{(2)}_{S,aS}(0)$ increases as the power is decreased and then eventually reaches a maximum value of ≈25 [see Fig. 4(c)].

The cross-correlation $g^{(2)}(\tau)$ is typically defined in terms of temporal correlations between intensities $I_1(t_1)$ and $I_2(t_2)$. Letting $I_1(I_2)$ to be the intensity of the Stokes radiation I_S (anti-Stokes radiation I_{aS}) and assuming stationary statistics, $g^{(2)}(\tau)$ is defined as follows:

$$g^{(2)}(\tau) = \frac{\langle I_S(0) I_{aS}(\tau)\rangle}{\langle I_S\rangle \langle I_{aS}\rangle}, \tag{2}$$

where $\tau = t_2 - t_1$ and the brackets indicate an ensemble average [16,17]. So long as the probabilities are low, it is straightforward to relate the ensemble averages to the probabilities of detection. For the unconditional probability of detecting a S photon, we can write

$$P(S, t_1)\Delta t_1 = C_S \langle I_S\rangle \Delta t_1, \tag{3}$$

where C_S accounts for the shape and efficiency of the S detector [17]. A similar expression follows for detecting an aS photon. For the joint probability, we have

$$\begin{aligned} &P(S, t_1, aS, (t_1+\tau))\Delta t_1 \Delta(t_1+\tau) \\ &\quad = C_S C_{aS} \langle I_S(t_1) I_{aS}(t_1+\tau)\rangle \Delta t_1 \Delta(t_1+\tau). \end{aligned} \tag{4}$$

This describes the joint probability of detecting a S photon at t_1 within Δt_1 and an aS photon at $(t_1 + \tau)$ within $\Delta(t_1 + \tau)$ [17]. Putting these expressions into the definition of $g^{(2)}(\tau)$ and letting $t_1 = 0$, we find that

$$g^{(2)}_{S,aS}(\tau) = \frac{P(S, aS, \tau)}{P(S)P(aS)} = \frac{P(S|aS, \tau)}{P(S)}, \tag{5}$$

from which the expression for $g^{(2)}(0)$ follows. Although pulsed lasers are not stationary, many of them can be treated as stationary sources that are deterministically modulated in time [18]. Then the peak heights in a pulsed $g^{(2)}(\tau)$ measurement carry the same information as a cw measurement, so long as the pulse duration is short compared to the coherence time of the signal [14].

As noted above for a pure SaS signal, $P(S|aS) \approx \eta_S$, which leads to $g^{(2)}_{S,aS}(0) = \eta_S/P(S) = \eta_S/(k_S P_L)$, where k_S is a constant describing the Stokes scattering strength and the collection and detection efficiencies. The correlation is therefore expected to increase with decreasing laser power as $1/P_L$. At very high powers, the probability of multiple S photons is no longer negligible, and the rate of accidental coincidences will rise [see Fig. 4(b)]. At very low powers, the SaS process is no longer much stronger than the spontaneously generated anti-Stokes, which leads to a maximum attainable $g^{(2)}_{S,aS}(0)$. This explains why the $1/P_L$ dependence is violated at low powers. Parra-Murillo *et al.* have modeled the behavior of $g^{(2)}_{S,aS}(0)$ for different thermal phonon occupation numbers and found that the behavior deviates from $1/P_L$ more strongly for higher numbers of thermal phonons [10]. In the absence of spontaneously generated anti-Stokes scattering, we would expect that $g^{(2)}_{S,aS}(0)$ will

increase without limit as power is reduced [10]. This implies that cooling the diamond will lead to a higher value of $g^{(2)}_{S,aS}(0)$.

In conclusion, by studying the correlations between Stokes and anti-Stokes photons as a function of laser pump power, we have shown that the second-order cross-correlation $g^{(2)}_{S,aS}(0)$ can be varied over a large range of values. We have discussed distinct processes for producing Stokes–anti-Stokes photon pairs: (1) uncorrelated photons from thermal phonons and (2) correlated photons from the SaS process. The relative strengths of these processes depend on experimental parameters (particularly pump power), as well as material properties. For quantum computing, the optimal material should be in the SaS regime for a large range of pump powers, which can be achieved, for example, by exploiting material resonances. Future work will therefore focus on developing engineered samples [19,20] with distinct resonances, such as optical cavities.

The authors acknowledge fruitful and stimulating discussions with P. Bharadwaj. A. J. acknowledges CAPES and ETH for financing his visit to ETH Zürich. L. N. thanks the Swiss National Science Foundation (SNF) for financial support through grant 200021-146358.

References

1. K. C. Lee, B. J. Sussman, M. R. Sprague, P. Michelberger, K. F. Reim, J. Nunn, N. K. Langford, P. J. Bustard, D. Jaksch, and I. A. Walmsley, Nat. Photonics **6**, 41 (2012).
2. D. G. England, P. J. Bustard, J. Nunn, R. Lausten, and B. J. Sussman, Phys. Rev. Lett. **111**, 243601 (2013).
3. K. C. Lee, M. R. Sprague, B. J. Sussman, J. Nunn, N. K. Langford, X.-M. Jin, T. Champion, P. Michelberger, K. F. Reim, D. England, D. Jaksch, and I. A. Walmsley, Science **334**, 1253 (2011).
4. K. F. Reim, P. Michelberger, K. C. Lee, J. Nunn, N. K. Langford, and I. A. Walsmley, Phys. Rev. Lett. **107**, 053603 (2011).
5. A. Kuzmich, W. P. Bowen, A. D. Boozer, A. Boca, C. W. Chou, L.-M. Duan, and H. J. Kimble, Nature **423**, 731 (2003).
6. C. H. van der Wal, M. D. Eisaman, A. André, R. L. Walsworth, D. F. Phillips, A. S. Zibrov, and M. D. Lukin, Science **301**, 196 (2003).
7. R. Chrapkiewicz and W. Wasilewski, Opt. Express **20**, 29540 (2012).
8. M. Bashkansky, F. K. Fatemi, and I. Vurgaftman, Opt. Lett. **37**, 142 (2012).
9. D. N. Klyshko, Sov. J. Quantum Electron. **4**, 1341 (1977).
10. C. A. Parra-Murillo, M. F. Santos, C. H. Monken, and A. Jorio, http://arxiv.org/abs/1503.01518.
11. J. Fan, A. Migdall, and L. J. Wang, Opt. Lett. **30**, 3368 (2005).
12. L. J. Wang, C. K. Hong, and S. R. Friberg, J. Opt. B **3**, 346 (2001).
13. K. Akiba, K. Kashiwagi, M. Arikawa, and M. Kozuma, New J. Phys. **11**, 013049 (2009).
14. O. A. Ivanova, T. S. Iskhakov, A. N. Penin, and M. V. Chekhova, Quantum Electron. **36**, 951 (2006).
15. Q. Glorieux, J. B. Clark, N. V. Corzo, and P. D. Lett, New J. Phys. **14**, 123024 (2012).
16. R. Loudon, *The Quantum Theory of Light* (Oxford University, 2010).
17. E. Wolf, *Optical Coherence and Quantum Optics* (Cambridge University, 1995).
18. H. Lajunen, J. Turunen, and P. Vahimaa, Opt. Express **11**, 1894 (2003).
19. E. Neu, P. Appel, M. Ganzhorn, J. Miguel-Sánchez, M. Lesik, V. Mille, V. Jacques, A. Tallaire, J. Achard, and P. Maletinsky, Appl. Phys. Lett. **104**, 153108 (2014).
20. A. Jorio, M. Kasperczyk, N. Clark, E. Neu, P. Malestinsky, A. Vijayaraghavan, and L. Novotny, Nano Lett. **14**, 5687 (2014).